

Fragmentation of Na_2^+ dimer ions in kilo-electron-volt collisions with He: A coupled wave-packet study

D. Babikov,^{1,2} F. Aguillon,¹ M. Sizun,¹ and V. Sidis¹

¹*Laboratoire des Collisions Atomiques et Moléculaires, Centre National de la Recherche Scientifique, URA No. 281, Bâtiment 351, Université Paris XI, 91405 Orsay Cedex, France*

²*Moscow Institute of Physics and Technology, Institutsky pereulok 9, Dolgoprudny, Moscow Region 141700, Russia*

(Received 22 June 1998)

The dynamics of the fragmentation of Na_2^+ dimer ions in keV collisions with He is investigated theoretically in the framework of the semiclassical coupled wave-packet method. The fast collisional motion is treated classically, whereas both the electronic motion and the vibrational or dissociative motion of the dimer are treated quantum mechanically. The frozen vibrational and rotational approximations are used to lighten the computational effort. The method is able to describe both the impulsive and electronic fragmentation mechanisms. The calculations are undertaken in a basis of 14 electronic states of the Na_2^+ -He system. Aside from the entrance $\Sigma_g 3s$ channel, the main contributions to the Na_2^+ fragmentation are those of the $\Sigma_u 3s$, $\Sigma_g 3p$, and $\Pi_u 3p$ channels. For each electronic state dissociation probabilities as functions of the impact parameter are presented for various dimer orientations to extract physical insight in the fragmentation mechanism. This analysis shows in particular that the contribution of the electronic mechanism is due to collisions where the He atom passes between the two Na nuclei. Doubly differential cross sections for dissociation are calculated for the $v=0$ initial state of the dimer and for the distribution of vibrational states. Good agreement with experiment is obtained assuming a small amount of initial vibrational excitation of the dimer. [S1050-2947(99)03101-7]

PACS number(s): 34.10.+x, 34.20.Mq, 36.40.Sx, 34.50.Lf

I. INTRODUCTION

Fragmentation of molecules or clusters by making them collide with atoms is a way of studying the dynamics of energy deposition and its subsequent distribution in polyatomic objects. Schematically, there are two main mechanisms by which collision-induced fragmentation can occur [1–3]. The first mechanism involves energy or momentum transfer from the relative collisional motion to internal vibrational and rotational degrees of freedom of the molecule (or cluster). If the transferred energy lies above the binding energy of an atom or a group of atoms in the molecule (or cluster) the latter may be freed and move apart. A particularly simple example of this mechanism is when the atomic projectile hits, in a close binary encounter, a specific atom or group of atoms in the molecule (or cluster) and kicks it out. This mechanism is called an *impulsive mechanism* [1–3]. Another simple example is when an initial binary kick is followed by successive caroms; the transferred energy is shared among several degrees of freedom of the molecule (or cluster), which may yield many-body fragmentation or delayed fragmentation as evaporation. The second mechanism involves an electronic transition to a dissociative or predissociative state of the molecule (or cluster), which automatically entails its fragmentation. Most known examples of such an *electronic mechanism* are those of dissociative charge exchange. The review of Ref. [4] and more recent works of Refs. [5,6] may help the reader trace the evolution of the experimental and theoretical investigations of this special case of molecular collisions.

A step forward in the experimental investigation of collision-induced fragmentation has been made recently by combined time-of-flight and multiparametric coincidence

techniques [1–3]. Applied to the study of Na_n^+ ($2 \leq n \leq 9$) cluster fragmentation in keV (laboratory energy) collisions with He this technique has made it possible to analyze how the impulsive and electronic mechanisms manifest themselves in the various $\text{Na}_{n-p}^+ + \text{Na}_p$ fragmentation pathways [2]. For the $\text{Na}_2^+ + \text{He}$ collision, which is the main subject of the present work, the latter experimental technique has made possible the complete measurement of all observables characterizing the collision-induced dissociation process. Such achievements are highly challenging for theory.

When considering the problem from a theoretical point of view, it should be kept in mind that a detailed *quantum-mechanical* description of translational-to-rovibrational energy transfer is far from being a trivial routine task in actual atom-molecule collision systems. The problem is dramatically complicated when dissociation and electronic transitions come, individually or together, into play. However, it has long been known that the use of classical or semiclassical approximations removes many of those difficulties and can provide, to a certain extent, reasonable descriptions of the dynamics of nuclei in a polyatomic system. This is the basis of the so-called *quasiclassical trajectory* (QCT) approach [7] also known as the *adiabatic molecular-dynamics* method (AMD) [8]. In that method all heavy particles in the collision system obey classical laws of motion under forces deriving from a unique Born-Oppenheimer potential-energy surface, usually that of the ground state. For nonadiabatic collisions, leading to electronic transitions (which are intrinsically quantum events), the QCT-AMD approach has to be modified. It is a very old idea that in such cases semiclassical treatments may be used in which the heavy particles move classically along prescribed trajectories while the electrons are treated quantum mechanically and obey a time-dependent Schrödinger

equation. The time dependence of the electronic problem is introduced by the classical motion of the heavy particles. Inasmuch as in such nonadiabatic collisions the system is simultaneously in several quantal electronic states, a unique potential governing the classical motion of the nuclei does not in principle exist. It has been suggested among other proposals [7,8] that the expectation value of the electronic Hamiltonian, determined by using the actual coherent superposition of the populated electronic states, could provide the unique potential sought. The interest of this proposal is that it ensures conservation of the total *average energy* of the system and thus introduces some energy transfer between classical and quantal degrees of freedom. While the method has met with some success in the calculation of integral cross sections for electronic transitions, it has known flaws when differential cross sections are considered. Namely, the scattering angle of the projectile and the kinetic energy of the heavy particles are independent of the actual quantal electronic state in which the system is. This is because the classical part of the system “knows” only the *average state* of its quantal part. While the scattering angle deficiency is a minor one in energetic collisions at small angles, the internal energy content of the molecule at the end of the collision is a serious issue especially when studying fragmentation. In a recent study of the $\text{Na}_2^+ + \text{He}$ collision-induced dissociation (CID) problem [3] such a method has been applied and its above-mentioned drawbacks have been met. An *ad hoc* “projection” procedure then had to be applied to patch up the theoretical treatment.

In the present work we revisit the problem of dimer fragmentation in the $\text{Na}_2^+ + \text{He}$ collision. From the outset, the internal vibration and electronic motions of the molecule are handled quantally in the framework of the *semiclassical coupled wave-packet technique* [5,6,9]. This approach has been designed originally to handle dissociative nonadiabatic molecular collisions and has been applied since to a variety of problems in molecular reaction dynamics at rather low energies [5,6,9,10]. The comparison of characteristic collisional and vibrational-rotational times then leads us to introduce a sudden approximation. The computation of transition amplitudes and differential cross sections of dissociation is described in this context. The results are compared with experiment and are scrutinized to gain more knowledge in the dissociation mechanisms.

The outline of the article is as follows. Section II sets up the theoretical framework. Section III deals with the method used to determine the relevant interaction potentials and couplings and presents some of their salient features. Section IV analyzes the results at various stages of the calculation and discusses the comparison with experiments. The main findings are summarized in Sec. V.

II. THEORETICAL FRAMEWORK

We consider the collision of the Na_2^+ dimer ion with He at $E_{\text{lab}} = 1 \text{ keV}$, i.e., $E_{\text{cm}} = 80 \text{ eV}$. Various relevant coordinates and parameters are shown in Fig. 1. Here $\vec{R}(t)$ is the relative vector between He and the center of mass of the dimer. The dimer vector \vec{r} is characterized by the bond length r and the orientation (θ, φ) in fixed space. The fixed space reference frame has its Z axis parallel to the incident

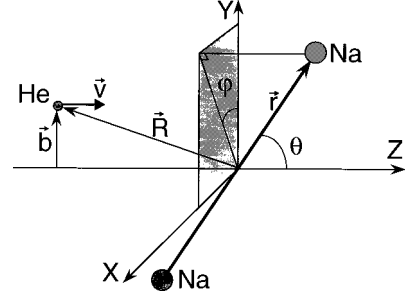


FIG. 1. Definition of the various space-fixed coordinates involved in the collision: $\vec{r} = (r, \theta, \varphi)$ is the Na_2^+ bond vector and \vec{R} is the relative $\text{Na}_2^+ - \text{He}$ vector. The axes are chosen with Z parallel to the initial relative velocity \vec{v} and Y parallel to the impact parameter vector \vec{b} .

direction of the relative velocity vector \vec{v} and its Y axis parallel to the impact parameter vector \vec{b} . The angle between the \vec{r} and $\vec{R}(t)$ vectors is denoted γ .

A. Principle equations of motion

Owing to the large reduced mass μ_{coll} of the $\text{Na}_2^+ - \text{He}$ collision system and the importance of the considered collision energy, the relative motion can be treated classically. For each impact parameter it is thus considered to evolve along a trajectory $\vec{R}(t)$. The total wave function of the system $\Psi(\{\vec{\rho}\}, \vec{r}, t)$ then depends on time via this trajectory and thus obeys the time-dependent Schrödinger equation

$$i \frac{\partial \Psi}{\partial t} = \left(-\frac{1}{2\mu} \Delta_{\vec{r}} + H_{\text{el}} \right) \Psi. \quad (1)$$

In the above $\{\vec{\rho}\}$ represents collectively the set of electronic coordinates, μ is the Na_2^+ reduced mass, and H_{el} is the electronic Hamiltonian of the system. Equation (1) expresses the quantal evolution of the rotational and vibrational motions of the molecule together with the electronic motion of the system along a prescribed trajectory $\vec{R}(t)$ to be specified below.

The corresponding rovibronic wave function can be expanded over a set of electronic basis functions $\phi_j(\{\vec{\rho}\}; r, \gamma, R)$ determined for fixed positions of the nuclei; the ϕ_j 's thus depend parametrically on the three relative coordinates r , γ , and R :

$$\Psi(\{\vec{\rho}\}, \vec{r}, t) = \sum_j P_j(t, \vec{r}) \phi_j(\{\vec{\rho}\}; r, \gamma, R). \quad (2)$$

Each $P_j(t, \vec{r})$ function constitutes a wave packet that describes the instantaneous rovibrational motion of the system in the j th electronic state. Substitution of expression (2) into Eq. (1) and projection onto the ϕ_j basis functions leads to a well-known set of coupled partial differential equations for the wave packets:

$$i \frac{\partial P_j(t, \vec{r})}{\partial t} = -\frac{1}{2\mu} \Delta_{\vec{r}} P_j(t, \vec{r}) + \sum_k H_{jk}(\vec{R}(t), \vec{r}) P_k(t, \vec{r}). \quad (3)$$

In the above we have made use of the notation

$$H_{jk}(\vec{R}(t), \vec{r}) \equiv \langle \phi_j | H_{\text{el}} | \phi_k \rangle_{\{\hat{\rho}\}} = H_{kj}(\vec{R}(t), \vec{r}). \quad (4)$$

Equation (3) actually assumes that the ϕ_j basis functions form a diabatic representation, i.e., that the $\langle \phi_j | d/dt | \phi_k \rangle_{\{\hat{\rho}\}}$ coupling matrix elements are sufficiently small to be neglected [11].

Following Ref. [12], the trajectory of relative collisional motion $\vec{R}(t)$ is obtained at each time t from the average potential

$$\tilde{V}(\vec{R}, \theta, \varphi) \equiv \sum_{j,k} \langle P_j(t, \vec{r}) | H_{jk}(\vec{R}(t), \vec{r}) | P_k(t, \vec{r}) \rangle_r \quad (5)$$

using Hamilton's equations

$$\dot{\vec{R}} = \frac{\vec{K}}{\mu_{\text{coll}}}, \quad \dot{\vec{K}} = -\vec{\nabla}_{\vec{R}} \tilde{V}. \quad (6)$$

While the use of a common trajectory to describe the scattering in all channels j is a rather crude procedure in general, it will be seen in Sec. IV A that it is legitimate in the present case because (i) when the electronic transitions are sizable they take place predominantly at small scattering angles where the trajectory does not matter very much and (ii) at large scattering angles where the impulsive mechanism is dominant, the system is predominantly in one electronic state (ground state ϕ_1). The use of a common trajectory to describe the scattering for all r values is justified by the fact that the r -average potential is very close to the actual r -dependent potential.

B. Sudden approximation

It has been rightly argued in Ref. [3] that, for the Na_2^+ -He collisions in the $E_{\text{cm}} \approx 10^2$ eV energy range, typical interaction times ($t_{\text{coll}} \approx 10^{-15} - 10^{-16}$ s) are at least one order of magnitude shorter than a typical vibration period of the Na_2^+ dimer, itself two orders of magnitude smaller than the typical Na_2^+ rotation period. Accordingly, the Na_2^+ dimer barely vibrates or rotates during the collision time. This has been checked in the early stages of the present work [13] by studying the hardest encounters when the He atom undergoes a head-on collision with a nucleus of the molecule. In the *most extreme* conditions investigated the molecule bond distance varied by less than 7% and its orientation by less than 5° over an interaction time of 100 a.u. ($\approx 2.4 \times 10^{-15}$ s). One can thus confidently make use of the sudden approximation in which the \vec{r} vector is considered as a *fixed parameter* during the collision [6,9]. As pointed out in Ref. [9], this essentially amounts to discarding the kinetic energy of the molecule in Eq. (3), i.e.,

$$i \frac{\partial P_j(t; \vec{r})}{\partial t} = \sum_k H_{jk}(\vec{R}(t); \vec{r}) P_k(t; \vec{r}). \quad (7)$$

The picture that emerges from this description is that of a quantum evolution of the electronic part of the problem, as a result of the classical relative atom-molecule motion, for fixed values of the parameter \vec{r} . Notwithstanding the latter frozen bond vector approximation, the molecule actually

gains momentum during the collision along its vibrational and rotational degrees of freedom; this will appear below.

C. Wave-packet analysis

From the solution of Eq. (7), one obtains for each impact parameter b the probability amplitudes $a_{jlm}(\varepsilon, b)$ that Na_2^+ dissociates in the electronic state j and the rotational state lm , with the dissociation energy ε :

$$a_{jlm}(\varepsilon, b) = \langle g_{\varepsilon jl}(r) Y_{lm}(\theta, \varphi) | P_j(t_{\text{final}}; r, \theta, \varphi) \rangle_{r, \theta, \varphi}. \quad (8)$$

$g_{\varepsilon jl}$ is the continuum wave function obeying the isolated molecule radial Schrödinger equation

$$\left(\frac{1}{2\mu} \frac{\partial^2}{\partial r^2} + \{H_{jj}(R \rightarrow \infty, r) - H_{jj}(R \rightarrow \infty, r \rightarrow \infty)\} + \frac{l(l+1)}{2\mu r^2} \right) g_{\varepsilon jl}(r) = \varepsilon g_{\varepsilon jl}(r). \quad (9)$$

Regardless of the rotational state of Na_2^+ , the dissociation probability density (i.e., probability per energy unit) is

$$\tau_j(\varepsilon, b) = \sum_{l,m} |a_{jlm}(\varepsilon, b)|^2. \quad (10)$$

To circumvent the tedious task of explicitly handling the rotation quantally, it is possible to approximate the exact $g_{\varepsilon jl}$ wave function in Eq. (9) by $g_{\varepsilon j \tilde{l}}(r)$, where \tilde{l} is a fixed value. Using this approximation together with the closure relation over the spherical harmonics leads to

$$\tau_j(\varepsilon, b) = \int \tau_j(\varepsilon, b; \theta, \varphi) \sin \theta \, d\theta \, d\varphi, \quad (11)$$

where

$$\tau_j(\varepsilon, b; \theta, \varphi) = |\langle g_{\varepsilon j \tilde{l}}(r) | P_j(t_{\text{final}}; r, \theta, \varphi) \rangle_r|^2. \quad (12)$$

In expression (12) the integration is carried out over r only. The validity of such an approximation requires the fixed \tilde{l} value to be representative of all the l components of $P_j(t_{\text{final}}; r, \theta, \varphi)$. The distribution of the l components may actually be very broad and it is generally not possible to find any representative value \tilde{l} of the whole final wave packet. The breadth of this distribution can be understood classically. If b , θ , and φ are such that there is a hard He- Na^+ core collision leading to a transfer of momentum perpendicular to the Na_2^+ bond, l becomes very large. Conversely, for the same impact parameter, if θ and φ are such that the He trajectory remains always far from the Na^+ cores, only a few rotational level will be populated and l is low. Hence the calculation of $\tau_j(\varepsilon, b; \theta, \varphi)$ according to Eq. (12) is expected to provide good results when \tilde{l} is the (θ, φ) -dependent classical value of the angular momentum

$$\tilde{l}^2(b; \theta, \varphi) = P_\theta^2 + \frac{P_\varphi^2}{\sin^2 \theta} \quad (13)$$

obtained from the classical equations of motion

$$\frac{dP_\theta}{dt} = - \left(\frac{\partial \tilde{V}}{\partial \theta} - \frac{P_\varphi^2 \cos \theta}{\mu \tilde{r}^2 \sin^3 \theta} \right), \quad \frac{dP_\varphi}{dt} = - \frac{\partial \tilde{V}}{\partial \varphi}, \quad (14)$$

where the average bond distance is defined similarly to Eq. (5),

$$\tilde{r}(t; \theta, \varphi) \equiv \sum_{j,k} \langle P_j(t; r, \theta, \varphi) | r | P_k(t; r, \theta, \varphi) \rangle_r. \quad (15)$$

Knowing $\tau_j(\varepsilon, b; \theta, \varphi)$, the differential cross sections for dissociation in each channel j for each orientation (θ, φ) may hence be obtained semiclassically as [14]

$$\sigma'_j(\varepsilon, \chi; \theta, \varphi) = \sum_\beta \frac{b_\beta \tau_j(\varepsilon, b_\beta; \theta, \varphi)}{\sin \chi \left(\frac{d\chi}{db} \right)_{b=b_\beta}}, \quad (16)$$

where use is made of the classical deflection function $\chi(b)$ stemming from Eq. (6). The sum in Eq. (16) extends to all branches β of the multivalued $\chi(b)$ function. Near the coalescence point of two branches (rainbow) we have resort to the textbook Airy function approximation [15]. Finally, the observable differential cross sections are obtained by the average of $\sigma'_j(\varepsilon, \chi; \theta, \varphi)$ over dimer orientations (θ, φ) :

$$\sigma_j(\varepsilon, \chi) = \int_0^\pi \sin \theta d\theta \int_0^{2\pi} \sigma'_j(\varepsilon, \chi; \theta, \varphi) d\varphi. \quad (17)$$

D. Implementation

Equation (7) is solved using an adapted version of the coupled wave-packet computer code of Refs. [6,10], which was designed to solve Eq. (3) for vibronic problems [i.e., cases when the molecule orientation is held fixed [9] or treated classically [6(b)]]. The set of equations (7) is obviously much less computationally demanding than those considered in the just cited literature. Further, significant computational efficiency can be gained by making the change of function

$$P_j(t; \vec{r}) = Q_j(t; \vec{r}) \exp\{i \eta_j(t; \vec{r})\}, \quad (18a)$$

with

$$\eta_j(t; \vec{r}) \equiv - \int_{t_{\text{initial}}}^t H_{jj}(\vec{R}(t'); \vec{r}) dt'. \quad (18b)$$

Indeed, while the P_j wave function can exhibit very-short-wavelength components in the r coordinate, especially when the collision gives rise to a large momentum transfer, the Q_j wave functions are always quite smooth and can be described with a large stepsize in the r grid.

Equation (7) then becomes

$$i \frac{\partial Q_j(t; \vec{r})}{\partial t} = \sum_{k \neq j} H_{jk}(\vec{R}(t); \vec{r}) \exp\{i[\eta_k(t; \vec{r}) - \eta_j(t; \vec{r})]\} Q_k(t; \vec{r}). \quad (19)$$

For a given impact parameter b and a molecule orientation (θ, φ) , the $Q_j(t; \{r\}, \theta, \varphi)$ and $\eta_j(t; \{r\}, \theta, \varphi)$ functions are determined simultaneously for a whole set $\{r\}$ of r values.

To solve Eqs. (7) and (19) we choose as the initial condition

$$P_j(t_{\text{initial}}; \vec{r}) = Q_j(t_{\text{initial}}; \vec{r}) = \delta_{j1} \chi_v(r). \quad (20)$$

Equation (20) specifies that the system is initially in the Na₂⁺ electronic ground state ϕ_1 and v th vibrational state χ_v . An isotropic initial rotational state is assumed for simplicity. It is noteworthy that Eqs. (7) and (19) may be made independent of the actual choice of χ_v . This is effected by writing

$$P_j(t; \vec{r}) = C_j(t; \vec{r}) \chi_v(r) = A_j(t; \vec{r}) \exp\{i \eta_j(t; \vec{r})\} \chi_v(r), \quad (21a)$$

$$C_j(t_{\text{initial}}; \vec{r}) = A_j(t_{\text{initial}}; \vec{r}) = \delta_{j1}, \quad (21b)$$

so that

$$i \frac{\partial A_j(t; \vec{r})}{\partial t} = \sum_{k \neq j} H_{jk}(\vec{R}(t); \vec{r}) \exp\{i[\eta_k(t; \vec{r}) - \eta_j(t; \vec{r})]\} A_k(t; \vec{r}). \quad (22)$$

Equations (21) and (22) are quite useful because the knowledge of the $C_j(t; \vec{r})$ functions provides the relevant $P_j(t; \vec{r})$ functions for arbitrarily chosen initial vibrational states $\chi_v(r)$, i.e., the calculations need not in principle be done for every χ_v taken into consideration.

Clearly, in the case of an electronically elastic collision [$H_{jk} \approx 0$ entailing $A_j(t; \vec{r}) \approx \delta_{j1}$] the effect of the collision is the accumulation of phase $\eta_1(t; \vec{r})$. This illustrates again that, although the \vec{r} vector is held fixed during the encounter, the molecule gains vibrational momentum, which in this case amounts to $\partial \eta_1(t; \vec{r}) / \partial r$.

E. Technicalities

The solutions of Eq. (22) for the quantum part of the problem and Eqs. (6) and (14) for the classical part are obtained in the following way. At each time t the propagation of Eq. (22) during the time step dt provides the values of the P_j wave packets at time $t + dt$. The average potential \tilde{V} is obtained using Eq. (5) and these updated values of P_j . With this potential Eqs. (6) and (14) are propagated during the time step dt .

To solve Eqs. (6) and (14) the Runge-Kutta integrator is used. The initial conditions are

$$\vec{R} = \begin{pmatrix} 0 \\ b \\ Z_{\text{initial}} \end{pmatrix}, \quad \dot{\vec{R}} = \begin{pmatrix} 0 \\ 0 \\ \sqrt{2E_{\text{coll}} / \mu_{\text{coll}}} \end{pmatrix}.$$

The impact parameter b is sampled over 120 equidistant values in the range $0 - 6a_0$. The starting point of He motion is $Z_{\text{initial}} = -12a_0$. The time of propagation is 700 a.u. From

the final velocity vector \vec{R}_{final} we obtain a classical scattering angle χ . The final rotational state \tilde{l} of the dimer is obtained from Eq. (13).

The propagation of the coupled equations [Eq. (22)] is done using a Lanczos scheme. The r grid is made of by 32 equidistant points in the interval $r \in [5.8a_0, 8.5a_0]$. Such a moderate number of points is a consequence of writing the wave packets in the form of Eqs. (18a) and (18b).

A total of 150 dimer orientations, corresponding to values of θ in the range 0° – 90° and φ in the range 0° – 180° were considered. The (θ, φ) grid was denser in the vicinity of $\theta = 90^\circ$ and $\varphi = 0^\circ$ because of the importance of this region for the impulsive mechanism.

III. POTENTIAL-ENERGY SURFACES AND COUPLINGS

In the present collision conditions only the outer electron of the Na_2^+ -He system is expected to eventually undergo excitation during the collision. This is expected from earlier studies of atom-atom systems such as Na-He and Na-Ne in similar conditions [16]. Accordingly, we have chosen to describe the effect of the two Na^+ cores of the dimer on the outer active electron using Na-centered l -dependent pseudo-potentials [17]. The spectator electrons of the He partner are explicitly considered in the calculation, although the corresponding orbitals are held frozen. The effect of He on the outer electron is not only a He-centered short-range (screened Coulomb-Hartree plus exchange) potential but also an orthogonality constraint imposed by the Pauli principle.

To build the diabatic representation required in the derivations presented in Sec. II we follow the lines of the already cited work on the Na-He and Na-Ne collisions [16]. The strictly diabatic basis obeying $\langle \phi_j | \partial/\partial R \text{ or } \partial/\partial \gamma | \phi_k \rangle = 0$ [11] would be made, in the present problem, of the orbitals of the isolated Na_2^+ dimer. To take into account the above-mentioned orthogonality constraint we make these orbitals orthogonal to the $1s_{\text{He}}$ orbital using the Schmidt procedure. In doing so, the orbitals are ordered with the $1s_{\text{He}}$ orbital first and then the Na_2^+ orbitals follow by order of increasing energy. While this procedure introduces slight $\partial/\partial R$ and $\partial/\partial \gamma$ coupling matrix elements, it was shown in Ref. [16] that these couplings are not important in the description of the electronic excitation process. It may be noted in passing that in the above we have not concerned ourselves with $\langle \phi_j | \partial/\partial r | \phi_k \rangle$ matrix elements since r enters the proposed dynamical treatment of Sec. II B only as a fixed parameter, as opposed to R and γ , which evolve during the encounter.

In practice the (nearly) diabatic basis considered is made of the lowest 14 eigenstates of the Na_2^+ molecule: $\Sigma_g^+ 3s$, $\Sigma_u^+ 3s$, $\Sigma_g^+ 3p$, $\Sigma_u^+ 3p$, $\Pi_u^+ 3p$, $\Pi_g^+ 3p$, $\Sigma_g^+ 3d$, $\Sigma_u^+ 3d$, $\Pi_u^+ 3d$, $\Pi_g^+ 3d$, $\Delta_g^+ 3d$, $\Delta_u^+ 3d$, $\Sigma_g^+ 4s$, and $\Sigma_u^+ 4s$. The Na_2^+ -He calculations are restricted to the A' irreducible representation of the C_s point group, that is, to states that are symmetric in the plane containing the three atoms. Excluding $A''(\Pi_{g,u}, \Delta_{g,u})$ states from the dynamics calculations amounts to making the approximation that Coriolis coupling, which arises from the tumbling of the triatomic plane, is negligible. Therefore, this approximation may have an effect on the Π and Δ states if at all.

The orbitals considered are expressed as linear combina-

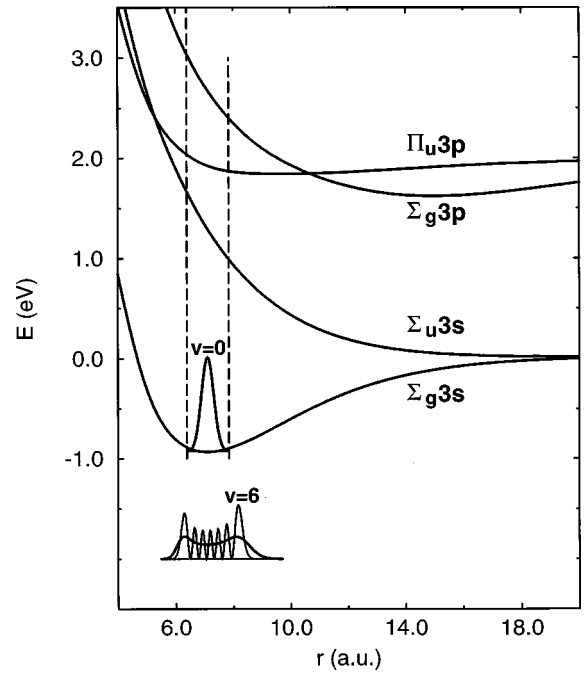


FIG. 2. Potential-energy curves of isolated Na_2^+ relevant to the present study. Superimposed on the ground-state curve is the probability density $|\chi_v|^2$ of the corresponding $v=0$ vibrational state. The related Franck-Condon zone is shown by dashed lines. The inset in the bottom of the figure shows the probability density for the $v=6$ vibrational level (oscillating curve) and for an incoherent superposition of vibrational states issued from the distribution of Sec. VI B (two-lobe curve).

tions of contracted Cartesian Gaussian-type orbitals (CGTOs) around each center. To the tabulated sets of basis orbitals of Ref. [17] we have added two d CGTOs, with exponents $\xi_d = 0.0155$ and $\xi'_d = 0.12$, around each Na center. The calculations of the Na_2^+ orbitals, the Schmidt orthogonalization, and the evaluation of the H_{jk} matrix elements [Eq. (4)] have been carried out using the GAMESS program [18]. The potential-energy curves of the isolated Na_2^+ dimer obtained in this way agree sufficiently well for the present purposes with the best data [19]. For example, for the ground state we get the equilibrium distance $r_e = 7.11a_0$ and potential well $D = 0.035$ hartree as compared to $r_e = 6.73a_0$ and $D = 0.036$ hartree in Ref. [19]. More generally, errors in the higher-energy curves do not exceed a few 10^{-3} hartree. The Na_2^+ potential-energy curves of the most significantly populated states in the Na_2^+ -He collision (Sec. IV) are shown in Fig. 2.

The $H_{jk}(r, \gamma, R)$ matrix elements have been determined for 20 relative orientations γ in the range 0° – 90° , 33 distances R in the range 0 – $12a_0$, and 15 bond distances r in the range $2a_0$ – $20a_0$. For values of γ in the range 90° – 180° the matrix elements could be obtained by symmetry. Three-dimensional interpolation of the data using bicubic splines [20] provide the H_{jk} matrix elements needed in the propagation of Eq. (19) or (22). In practice, to avoid spline undulations in regions near the cores where the potential varies rapidly, it has been found most convenient to interpolate the logarithm of the data rather than the data themselves.

Figure 3(a) shows the entrance $\text{Na}_2^+(\Sigma_g^+ 3s) + \text{He}$ potential-energy surface $H_{11}(r, \gamma, R)$ for one fixed value of the r coord-

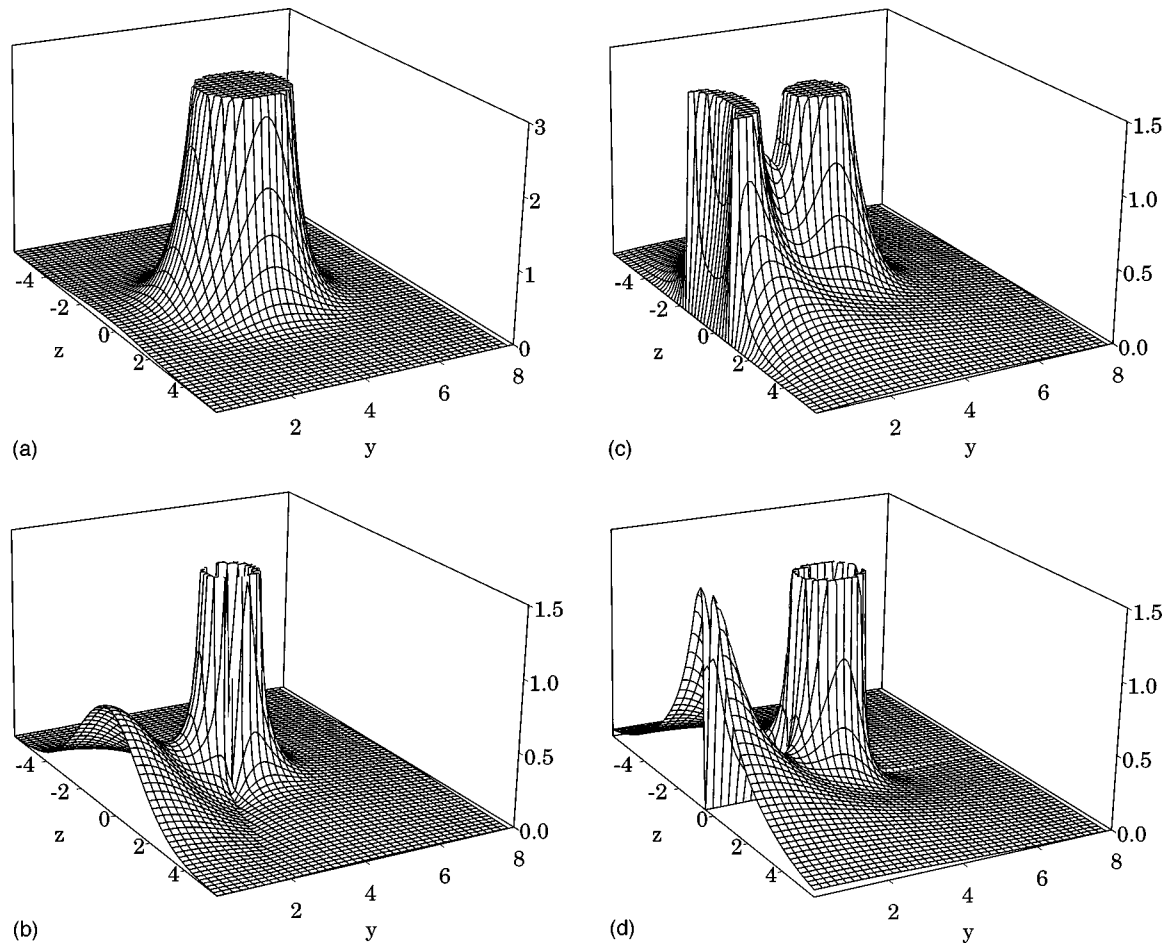


FIG. 3. (a) Entrance $\text{Na}_2^+(\Sigma_g 3s)$ -He potential-energy surface $H_{11}(r, \gamma, R)$. Shown is the potential in the half (Y, Z) plane defined in Fig. 1 when the Na_2^+ dimer (with $r = r_e = 7.11a_0$) is placed along the Y axis. Energy and distances are in atomic units. (b)–(d) Coupling to energy difference ratios $|H_{1j}/(H_{jj} - H_{11})|$ for the interaction between the $\Sigma_g 3s$ entrance state and some excited electronic states of the Na_2^+ -He system: (b) $\Sigma_g 3s$ - $\Sigma_g 3p$, (c) $\Sigma_g 3s$ - $\Sigma_u 3s$, and (d) $\Sigma_g 3s$ - $\Pi_u 3p$. The arrangement of the dimer is the same as in (a).

dinate equal to the equilibrium distance r_e of the isolated Na_2^+ dimer. The highest energy in this figure was chosen to be equal to the collision energy ($E_{\text{cm}} = 80 \text{ eV} \approx 2.94 \text{ a.u.}$). It shows that the classically forbidden region is a sphere with radius $\approx 1a_0$ centered at the position of the Na^+ core ($r/2 = r_e/2 \approx 3.55a_0$). Another noticeable feature of this figure is that there is a lot of room between the Na^+ cores where the He atom can easily pass through. It should be noted that for the energy scale of the figure, all the other $H_{jj}(r, \gamma, R)$ potentials look nearly the same. This justifies the approximation that a common potential may be used to treat the encounter.

Figures 3(b)–3(d) show samples of $|H_{1j}(r, \gamma, R)/[H_{jj}(r, \gamma, R) - H_{11}(r, \gamma, R)]|$ functions for fixed $r = r_e$ ($r/2 \approx 3.55a_0$). The importance of the coupling to the energy difference ratio is a measure of the likeliness of a transition. It is seen that excluding the classically forbidden region [see Fig. 3(a)], these ratios are sizable in the region between the Na^+ cores and not outside. Electronic excitation is thus expected to occur for collision trajectories that pass in between the cores. Figure 3(a) indicates that such trajectories correspond to soft collisions in which the trajectory should not be deflected significantly. Another interesting feature of Figs. 3(b)–3(d) is that the $|H_{1j}/(H_{jj} - H_{11})|$ ratios reflect, actu-

ally through H_{1j} , characteristics of the interacting Na_2^+ electron clouds: the $\Sigma_g 3s$ - $\Sigma_g 3p$ interaction builds around the Na-Na axis and maximizes halfway between the cores; the $\Sigma_g 3s$ - $\Sigma_u 3s$ interaction also builds along the Na-Na axis but, owing to symmetry, it vanishes and changes sign midway; the $\Sigma_g 3s$ - $\Pi_u 3p$ interaction builds between the Na^+ cores but off axis. Finally, it may also be noted that the $\Sigma_g 3s$ and $\Sigma_u 3s$ potential surfaces undergo a diabatic crossing that appears in Fig. 3(c) as a truncated hollowed out cylinder. This is somewhat reminiscent of a similar feature in the He- H_2 system [21].

IV. RESULTS

Results will first be presented for the collision-induced dissociation (impulsive mechanism) and dissociative electronic excitation (electronic mechanism) for Na_2^+ ions in their ground vibrational state. The case of vibrationally hot Na_2^+ ions will be examined next. It is generally found that four electronic states among the considered 14 (Sec. III) are populated significantly, namely, the $\Sigma_g 3s$ ground state and the $\Sigma_u 3s$, $\Sigma_g 3p$, and $\Pi_u 3p$ states.

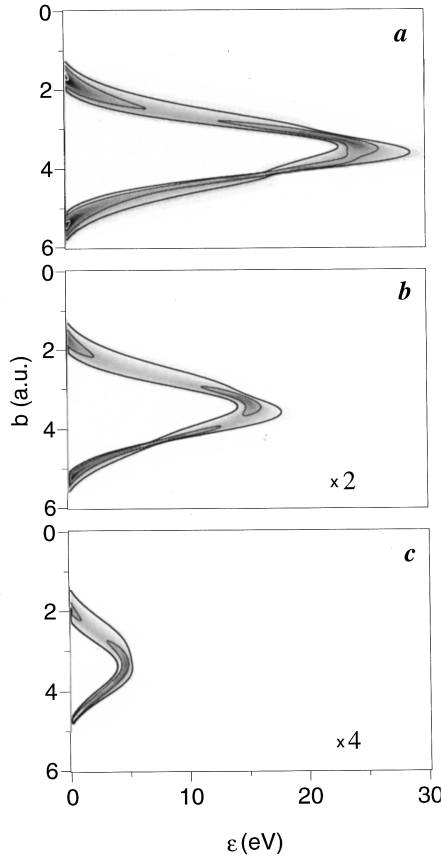


FIG. 4. Contour maps of the probability density $\tau_1(\varepsilon, b; \theta, \varphi)$ of dissociation in the entrance electronic state $\phi_1(\Sigma_g 3s)$ as a function of the energy ε of the fragments and the impact parameter b . Different azimuthal orientations of the dimer are shown for $\theta = 90^\circ$: (a) $\varphi = 0$, (b) $\varphi = 10^\circ$, and (c) $\varphi = 20^\circ$. The scale of (c) is bigger than those of (b) and (a) by the indicated factors. Darker areas indicate higher intensities.

A. Vibrationally cold Na_2^+ dimer

1. Fragmentation in the electronic ground state

From the probability amplitude $P_1(t_{\text{final}}; \vec{r})$ that the system remains in the electronic ground state $\phi_1(\Sigma_g 3s)$ one obtains [Eq. (12)] the probability density $\tau_1(\varepsilon, b; \theta, \varphi)$ of dissociation with an energy ε of the fragments as a function of impact parameter b and dimer orientation (θ, φ) . Figures 4(a)–4(c) show this function for $\theta = 90^\circ$ and a few azimuthal angles φ . It is seen [Fig. 4(a)] that the largest fragmentation energy occurs for the orientation $\theta = 90^\circ$ and $\varphi = 0^\circ$ at $b = \tilde{r}/2 \approx 3.5a_0$. The probability density in this range maximizes near the value of the relative energy of the fragments one gets classically for a binary, hard-sphere-type, head-on collision of one Na^+ core of the dimer with the He atom:

$$\begin{aligned} \varepsilon_{\text{max}}^{\text{cl}} &= \left(\frac{m_{\text{He}}}{m_{\text{He}} + m_{\text{Na}}} \right)^2 E_{\text{lab}} = \frac{m_{\text{He}}(m_{\text{He}} + 2m_{\text{Na}})}{(m_{\text{He}} + m_{\text{Na}})^2} E_{\text{cm}} \\ &= 21.9 \text{ eV}. \end{aligned} \quad (23)$$

It also establishes once more that although the dimer can barely move during the collision, it acquires momentum that makes the dimer dissociate in the postcollision stage.

Collisions with smaller and larger impact parameters than $b = \tilde{r}/2 \approx 3.5a_0$ produce two similar branches of the $\tau_1(\varepsilon, b; \theta, \varphi)$ probability density. Dissociation does not occur for $b \leq 1.2a_0$ and $b \geq 5.6a_0$. For these ranges of impact parameters the He atom passes at distances larger than $2a_0$ from a Na^+ core and the transferred momentum is insufficient to vibrationally excite the dimer up to dissociation.

The evolution of the dissociation probability density with φ for $\theta = 90^\circ$ [Figs. 4(a)–4(c)] shows that the maximum energy of the fragments, as well as the corresponding impact parameter, decreases as the dimer axis is twisted out of the collision plane. As φ increases, the smallest distance of approach of a Na^+ core to He increases, thereby reducing the momentum transfer to the dimer. For $\varphi > 30^\circ$ this smallest distance of approach becomes larger than $2a_0$ and no dissociation in the $\Sigma_g 3s$ state is possible any longer.

More generally, the evolution with orientation of the impact parameter dependence of the dissociation probability density can be roughly deduced from Figs. 4(a)–4(c), keeping in mind the image that the He atom has to fall within a sphere, centered around one Na^+ core, of radius $\approx 2a_0$; the closer the He atom gets to the center of the sphere the larger the transferred momentum and the relative energy of the fragments. Thence the decrease of θ from 90° holding $\varphi = 0$ will give rise to a pattern, similar to Fig. 4(a), except that the maximum fragmentation energy moves to smaller b values. This is understood with the above-discussed picture: The center of the sphere is hit for an impact parameter $b = \tilde{r}/2 \sin \theta$. Of course, θ should not be too small for the other Na^+ core to be disregarded.

Let us briefly mention that a kinematic event has been erased artificially from Fig. 4. This is the very specific case when the He atom bounces off one Na^+ core and then faces the second one. This case occurs for a very narrow range of impact parameters and gives rise to much larger fragmentation energies than those considered experimentally [Fig. 9(a)]. In the final cross-section calculation (Sec. IV A 4) this effect is actually included, but cannot be seen in the (ε, χ) window considered.

2. Dissociative electronic excitation

As in Sec. IV A 1, the probability density $\tau_j(\varepsilon, b; \theta, \varphi)$ of dissociation (with energy ε of the fragments as a function of impact parameter b for orientation θ and φ) when the system has undergone an electronic excitation $\phi_1 \rightarrow \phi_j$ is obtained from the computed probability amplitude $P_j(t_{\text{final}}; \vec{r})$ using Eq. (12). It is found that the $\Sigma_g 3p$, $\Sigma_u 3p$, and $\Pi_u 3p$ states are systematically far more populated than the other electronic states considered (Sec. III).

Figures 5(a)–5(c) show the dissociation probability densities for these states as functions of impact parameter at the fixed orientation $\theta = 90^\circ$ and $\varphi = 0^\circ$. The whole pattern is concentrated in the small-impact-parameter range $0 \leq b \leq 2a_0$. From Fig. 3 and Sec. III it is obvious that the electronic excitation takes place when the trajectory of the He atom passes in between the Na^+ cores. The symmetry characteristics of the electron clouds, already discussed in Sec. III, also reflect themselves in the plots of Figs. 5(a)–5(c). Thus, for $b \approx 0$, $\theta = 90^\circ$, and $\varphi = 0^\circ$, the $(\text{HeNa}_2)^+$ system forms an isosceles triangle that transforms according

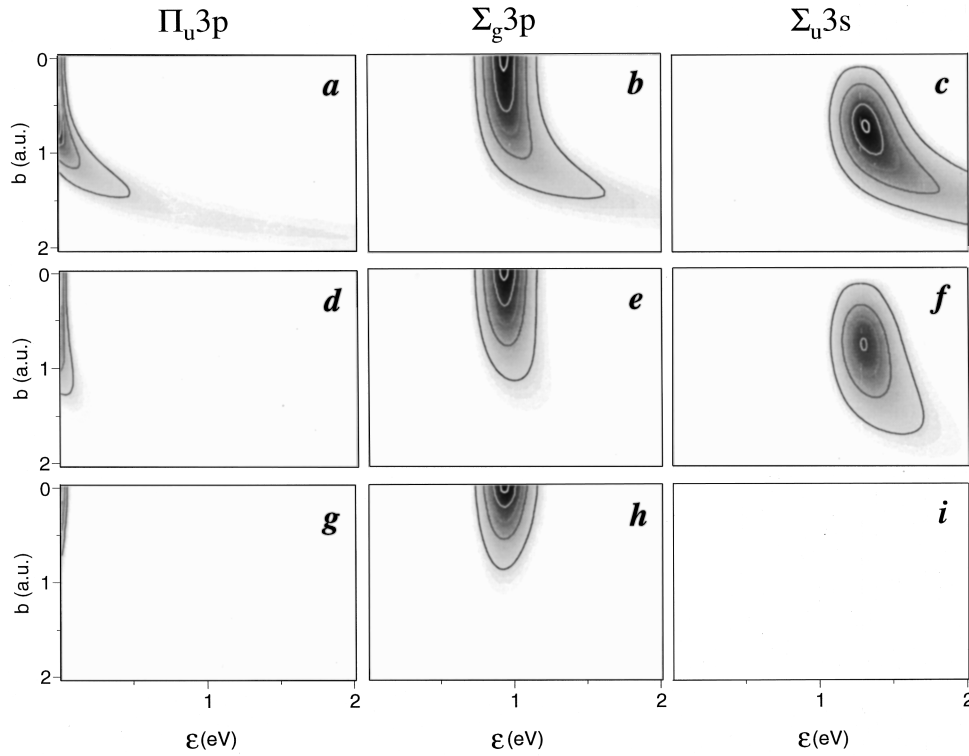


FIG. 5. Contour maps of the probability density $\tau_j(\varepsilon, b; \theta, \varphi)$ of dissociation in the excited electronic states ϕ_j ($\Sigma_u 3s$, $\Sigma_g 3p$, and $\Pi_u 3p$) as a function of the energy ε of the fragments and the impact parameter b . Different azimuthal orientations of the dimer are shown for $\theta = 90^\circ$: (a)–(c) $\varphi = 0^\circ$, (d)–(f) $\varphi = 30^\circ$, and (g)–(i) $\varphi = 90^\circ$. Darker areas indicate higher intensities.

the C_{2v} symmetry point group. For such an arrangement the $\Sigma_g 3p$ and $\Pi_u 3p$ states have the same A_1 symmetry as the entrance $\Sigma_g 3s$ state and can thus be populated at $b = 0$; the $\Sigma_u 3s$ state having B_2 symmetry cannot. On the other hand, as soon as b becomes different from zero these selection rules disappear. Indeed, the $(\text{HeNa}_2)^+$ system has then planar symmetry only (C_s point group); the $\Sigma_g 3s$ and $\Sigma_u 3s$ states now belonging to the same A' irreducible representation may thus interact [see Fig. 3(c)]. This is nicely illustrated in Fig. 5.

The ε ranges characterizing the dissociative electronic excitation processes are governed by vertical transitions as a result of the sudden collision conditions discussed in Sec. II B. At the smallest impact parameters they are roughly determined by the Franck-Condon zone and the related reflection principle [7]. Accordingly, the closeness to $\varepsilon \approx 0$ of the $\Pi_u 3p$ structure is a consequence of the particular shape of the corresponding Na_2^+ potential-energy curve in the Franck-Condon region (Fig. 2). The positions of the $\Sigma_g 3p$ and $\Sigma_u 3s$ structures at $\varepsilon \approx 1$ eV are consistent with this interpretation scheme as well.

When the impact parameter increases beyond $b \approx 0.8a_0$ the patterns clearly depart from the Franck-Condon expectation. This is due to the closer passage of the He atom to one of the Na^+ cores: The larger the b , the closer this encounter and the larger the transferred momentum. Hence the observed tails extending towards large ε values in the patterns of Figs. 5(a)–5(c) are nothing but a manifestation of the impulsive mechanism in the electronically excited channels.

Figures 5(a)–5(i) show the evolution of the $\Pi_u 3p$, $\Sigma_g 3p$, and $\Sigma_u 3s$ dissociation probability densities as functions of

impact parameter for $\theta = 90^\circ$ when φ increases. As was the case in Sec. IV A 1, one observes the progressive reduction of the impulsive tails. The progressive extinction of the $\Sigma_u 3s$ process as φ approaches 90° [Figs. 5(c)–5(f), and 5(i)] has again to do with symmetry: For $\varphi = 90^\circ$ the $(\text{HeNa}_2)^+$ system keeps a T shape (isosceles triangle) for all impact parameters. As argued above as well as in Sec. III, the $\Sigma_g 3s$ and $\Sigma_u 3s$ states having respectively A_1 and B_2 symmetry in this arrangement do not interact.

3. Comparison of the dissociation mechanisms

Figure 6 gathers the $\tau_j(\varepsilon, b; \theta, \varphi)$ dissociation probability densities for the ground $\Sigma_g 3s$ and excited $\Sigma_u 3s$, $\Sigma_g 3p$, and $\Pi_u 3p$ processes at $\theta = 90^\circ$ and $\varphi = 0^\circ$. The $\Sigma_g 3s$ process results exclusively from the impulsive mechanism and is characterized by the two branches around $b \approx \bar{r}/2$. The $\Sigma_g 3p$ and $\Sigma_u 3s$ structures appear in a close (ε, b) neighborhood. Their impulsive tails are seen to merge and display asymptotically the same slope as the $\Sigma_g 3s$ purely impulsive process. It is clearly seen from this figure that the dissociative electronic excitation and impulsive dissociation (whether in the ground or excited states) take place in distinct impact parameter ranges.

4. Differential cross sections for dissociation

In practice, it is not the $\tau_j(\varepsilon, b; \theta, \varphi)$ functions that are accessible to experiment but rather the doubly differential cross section in the scattering angle of the projectile χ and the relative energy of the fragments ε [Eq. (16)]. The transformation of the τ_j functions into the σ_j ones is achieved

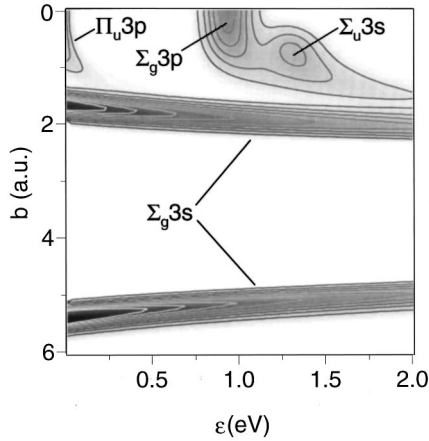


FIG. 6. Contour maps of the probability density $\tau(\varepsilon, b; \theta, \varphi)$ of dissociation summed over all electronic channels j as a function of the energy ε of the fragments and the impact parameter b for $\theta = 90^\circ$ and $\varphi = 0$.

through Eqs. (16) and (17). Figure 7 shows samples of deflection functions $\chi(b; \theta, \varphi)$ that enable one to effect the latter transformation. For a given orientation (θ, φ) of the dimer two impact parameters contribute to the same χ ; the two impact parameters merge into a single value at a limiting χ value. This is handled along the lines of the discussion following Eq. (16). Figure 8 shows examples of the way these rainbow features contribute to the cross section for dissociation in $\Sigma_g 3s$ ground state.

Figure 9(b) shows the final cross section for dissociation including all important processes: $\Sigma_g 3s$, $\Sigma_u 3s$, $\Sigma_g 3p$, and $\Pi_u 3p$. In this figure one can easily distinguish three main structures, corresponding to different channels of dissociation. As expected from Figs. 6 and 7, the dissociation in the $\Sigma_g 3s$ electronic state appears at large scattering angles ($\chi \geq 20^\circ$) and displays a trend similar to the impulsive structure of the experimental cross section [Fig. 9(a)]. Dissociative electronic excitation takes place at small scattering angles ($\chi \leq 10^\circ$): Excitation of the $\Pi_u 3p$ weakly bound state forms a structure at the $(\varepsilon \approx 0, \chi \approx 0)$ region, while the $\Sigma_u 3s$ and

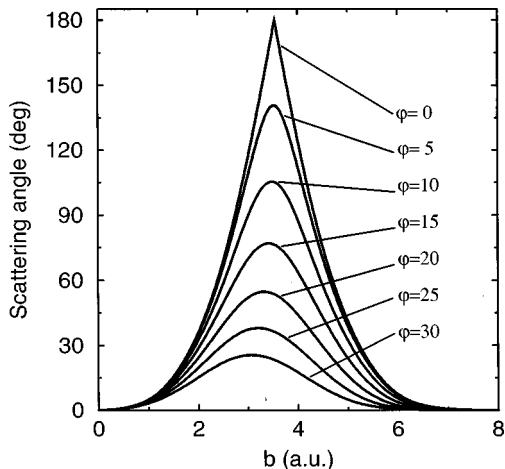


FIG. 7. Classical scattering angle $\chi(b; \theta, \varphi)$ determined from the classical relative motion as a function of impact parameter b for dimer orientations defined by $\theta = 90^\circ$ and different φ values indicated in the figure.

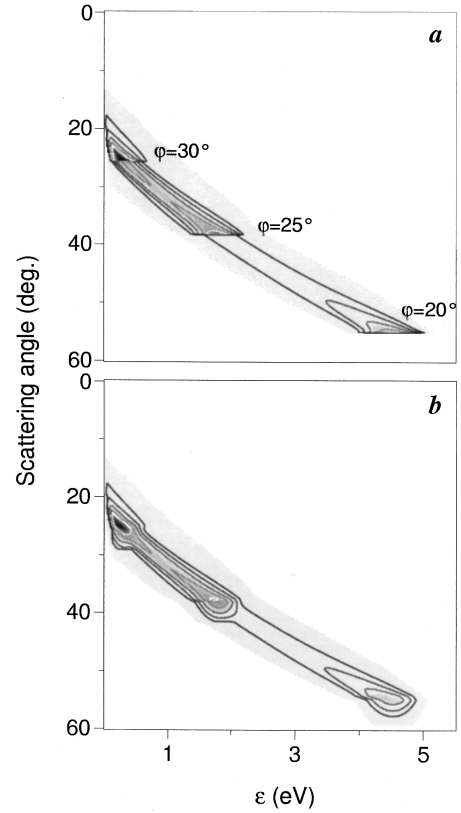


FIG. 8. Contour maps showing the $\sigma'_1(\varepsilon, \chi; \theta, \varphi)$ contributions of the dimer orientations $\theta = 90^\circ$ and $\varphi = \{20^\circ, 25^\circ, 30^\circ\}$ to the doubly differential cross section $\sigma_1(\varepsilon, \chi)$ [see Eq. (17)] for dissociation in the entrance state $\phi_1(\Sigma_g 3s)$: (a) classical cross section with diverging rainbows and (b) result of the treatment of the rainbow regions by Airy functions. Darker areas indicate higher intensities.

$\Sigma_g 3p$ states are responsible for the structure at $\varepsilon \approx 1 - 1.3$ eV. The general appearance of the plot shows many qualitative similarities to the experimental data of Refs. [1,3] presented in Fig. 9(a).

B. Case of vibrationally excited Na_2^+ dimers

Though the $v=0$ cross section of Sec. IV A [Fig. 9(b)] bears a qualitative resemblance to the experimental data of Refs. [1,3] [Fig. 9(a)], a few differences are noticeable. First, the computed $\Sigma_g 3s$ impulsive contribution extends too much towards high ε values as compared to experiment where it exhibits greater localization around its maximum near $\varepsilon \approx 0.2$ eV. Second, instead of the distinct structures $\Sigma_g 3p$ and $\Sigma_u 3s$, appearing, respectively, at $\varepsilon \approx 1$ and 1.3 eV in the theory, the experiment shows a single structure at $\varepsilon \approx 0.9$ eV. Actually, the above comparison disregards the fact that in the experimental conditions the Na_2^+ dimer ions have a vibrational state distribution $w(v)$ and so the actual cross section results from an incoherent superposition of initial vibrational states

$$\langle \sigma(\varepsilon, \chi) \rangle = \sum_v w(v) \sigma^v(\varepsilon, \chi). \quad (24)$$

In Eq. (24) $\sigma^v(\varepsilon, \chi)$ is the doubly differential dissociation cross section for each vibrational state v initially present in

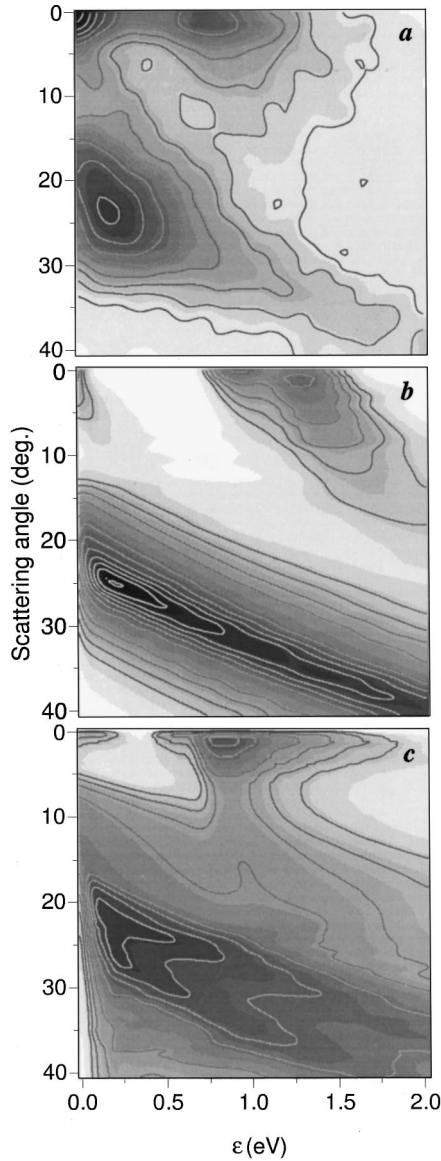


FIG. 9. Contour maps of the doubly differential cross section $\sigma(\varepsilon, \chi)$ for dissociation irrespective of the final electronic state: (a) experimental result of Refs. [1,3], (b) cross section $\sigma(\varepsilon, \chi)$ obtained for Na₂⁺ assumed to be initially in the ground vibrational state, and (c) cross section $\langle \sigma(\varepsilon, \chi) \rangle$ for the distribution of vibrational states of Na₂⁺ discussed in the text. Darker areas indicate higher intensities.

the Na₂⁺ beam. Yet the actual vibrational state distribution $w(v)$ is unknown. An average internal energy ≈ 0.2 eV of the dimer ions was tentatively proposed in Ref. [3] to make the simple binary encounter kinematics model of impulsive dissociation reproduce the overall trend of the experimental data. This value seemed to receive support from more involved classical trajectory calculations [3]. Still, as such, this estimate is insufficient to make the evaluation of a formula such as Eq. (24) possible. We have thus proceeded as described below.

The Na₂⁺ dimer ions are produced in the experiment of Refs. [1,3] by the bombardment of a Na₂ neutral beam by fast (40-eV) electrons. Thus the $w(v)$ distribution is merely reflecting, through the Franck-Condon principle, the vibrational distribution $w_0(v_0)$ in the parent Na₂ neutral beam:

$$w(v) = \sum_{v_0} w_0(v_0) |\langle \chi_v | \chi_{v_0}^0 \rangle|^2, \quad (25)$$

where χ_v and $\chi_{v_0}^0$ are, respectively, vibrational wave functions of the ionized and neutral dimers. In the experimental conditions of Refs. [1,3] the neutral Na₂ dimers are likely to have v_0 in Eq. (25) bounded by $v_0 \leq 2$. For simplicity, we make the working assumption that

$$w(v) \approx |\langle \chi_v | \chi_{v_0=0}^0 \rangle|^2. \quad (26)$$

It has occurred that the maximum of this distribution is located near $v=6-7$ and its width at half maximum encompasses states in the range $3 \leq v \leq 10$. Its mean vibrational energy

$$\langle E_{\text{vib}} \rangle = \sum_v w(v) E_v \quad (27)$$

is $\langle E_{\text{vib}} \rangle = 0.096$ eV. In Fig. 2 we compare the initial distribution of r values for the corresponding incoherent superposition of vibrational states to the initial probabilities $|\chi_v|^2$ for $v=0$ and 6 vibrational levels.

We have determined the $\sigma^v(\varepsilon, \chi)$ cross sections for v in the interval $v \in [3, 10]$ as described in Sec. II C Eqs. (21) and (22), using the relevant $P_1 = \chi_v$ initial vibrational wave functions. The corresponding average [Eq. (24)] over the distribution $w(v)$ [Eq. (26)] is displayed in Fig. 9(c). The result definitely improves the comparison with experiment. The $\Sigma_g 3s$ impulsive structure is now more concentrated in a narrower ε range than Fig. 9(b) and the $\Sigma_g 3p$ and $\Sigma_u 3s$ structures have merged into a single one properly located at 0.9 eV. While all details of the new pattern do not have a general straightforward explanation, the way in which the electronic structures have evolved has a transparent interpretation. As seen from Fig. 2, the $\Sigma_u 3s$ energy curve is more repulsive than the $\Sigma_g 3p$ one. Dissociation energies in *vertical* electronic transitions are thus more sensitive in the former than in the latter case to the r location where the transition takes place. Moreover, the vibrationally excited states can roughly be viewed as essentially made of two lobes placed around the turning points of classical motion (see Fig. 2). Actually, the outer lobe gives rise more efficiently to an electronic transition than the inner lobe. This is most probably related to the smaller energy difference for the electronic transition at the outer lobe than at the inner one. These characteristics are sufficient to explain why the $\Sigma_g 3p$ and $\Sigma_u 3s$ structures move to lower dissociation energy with vibrational excitation and the more so for the latter than for the former.

The comparison with experiment still indicates that the breadth and intensity of the structure at $\varepsilon \approx 0$ and $\chi \approx 0$, which actually originate from dissociation in the $\Pi_u 3p$ state (Sec. IV A 2), are rather underestimated in the calculation. Again, this issue can be examined in terms of vertical transitions from the electronic ground state. Two possible explanations related to the comparative flatness of the $\Pi_u 3p$ energy curve in the Franck-Condon region of the distribution of vibrational states considered can be proposed: (i) Higher accuracy of this curve than what was considered reasonable in Sec. III can change the relative importance of what goes

into (bound) vibrational excitation and dissociation in this state or (ii) a different vibrational distribution emphasizing small- r values further can yield more dissociation. Another possibility could lie in one of the approximations made in Sec. II to lighten the computational effort. More specifically, it is not clear by now what the effect of disregarding Coriolis coupling in the present work (Sec. III) could have on the discrepancy discussed.

V. SUMMARY AND CONCLUSION

One of the incentives to undertake the present work was to apply a state-of-the-art method for treating the dynamics of Na_2^+ fragmentation in collisions with He, a process that has been the subject of a detailed experiment in Refs. [1,3]. From the latter study it appeared that fragmentation can occur with different characteristics either as a vibrational excitation above the dissociation limit in the initial electronic ground state of Na_2^+ or as a result of an electronic excitation to a dissociative state. This implied the use of a nonadiabatic molecular collision framework to treat the corresponding dynamics. The semiclassical coupled wave-packet approach that treats *electronic* and *vibrational* (whether bound or dissociative) *motions quantally* and the remaining motions classically is to date the most developed theory of that kind. Yet this method is computationally quite demanding, especially in the collision energy range in which the experiments of Refs. [1,3] have been carried out. It turns out that for the latter collision conditions one can advantageously make use of an approximation in which the dimer neither vibrates nor rotates *during the encounter*. This approximation has actually made the present work affordable. While the dimer is held frozen, as just stated, it actually accumulates momentum and may actually undergo electronic transitions as the He atom passes by. This accumulated momentum reveals itself in a *postcollisional stage* and contributes to the final vibrational- (eventually dissociative) rotational motions of the dimer in each of the final electronic state produced by the collision. In the work reported the information on the accumulated vibrational momentum of the dimer is contained in the bond length dependences of the electronic transition probability amplitudes. Likewise, the information on the accumulated rotational angular momentum is contained in the dependences of these electronic amplitudes upon the orientation of the dimer. Nevertheless, to simplify the computation we have extracted this information from classical equations of motion as discussed in Sec. II C.

It may be stated right away that the reported results confirm the analysis of Refs. [1–3] of the different structures observed in the experimental fragmentation cross section. Conversely, the general agreement of the present results, taking a plausible initial vibrational distribution of the Na_2^+ ions into account, with experiment is in strong support of the cogency of our theoretical treatment. From this agreement we are inclined to infer that the Na_2^+ ions in the experiment of Refs. [1,3] were cooler than what was initially thought.

Concerning the fragmentation mechanism, collisions leaving the Na_2^+ dimer ion in its electronic ground state $\Sigma_g^+ 3s$ lead to dissociation at large scattering angles ($\chi \geq 20^\circ$). This corresponds to important momentum transfer, justifying its designation as impulsive mechanism in Refs. [1–3]. The momentum transfer actually occurs most efficiently when the He trajectory passes close to one of the Na^+ cores: typically within a sphere of radius $\approx 2a_0$. Most salient features and trends of this CID mechanism correspond to what may be predicted from classical mechanics. Details such as the shape, breadth, and importance of dissociation probability densities actually depend on the initial quantal state and quantal projection.

Collisions that bring the Na_2^+ dimer in an excited electronic state ($\Sigma_u^+ 3s$, $\Sigma_g^+ 3p$, and $\Pi_u^+ 3p$) occur for He trajectories going into the region between the nuclei and thus contribute mainly to relatively small scattering angles. For these dissociative electronic excitation processes the gross features of the probability densities correspond to what may be predicted from Franck-Condon overlaps between the initial vibrational state and the final dissociation continuum. Still finer details, for instance, the extension of dissociative electronic excitation structures by impulsive tails, arise from the detailed dependence of the electronic transition probability amplitudes upon the Na_2^+ bond distance.

Further work on collision-induced fragmentation of larger alkali-metal cluster ions, such as $\text{Na}_3^+ + \text{He}$ [2], should show which aspects of the present semiclassical treatment will survive the dimensionality increase of the system.

ACKNOWLEDGMENTS

This work was initiated in the frame of the EU Human Capital and Mobility Program through the Collision Induced Cluster Dynamics Network under Contract No. CHRX-CT-940643. We would like to thank J. A. Fayeton, M. Barat, and Y. J. Picard at LCAM (Orsay) for providing their experimental data and for very helpful discussions.

-
- [1] J. C. Brenot, H. Dunet, J. A. Fayeton, M. Barat, and M. Winter, Phys. Rev. Lett. **77**, 1246 (1997).
 [2] M. Barat, J. C. Brenot, H. Dunet, and J. A. Fayeton, Z. Phys. D **40**, 323 (1997).
 [3] J. A. Fayeton, M. Barat, J. C. Brenot, H. Dunet, Y. J. Picard, U. Saalman, and R. Schmidt, Phys. Rev. A **57**, 1058 (1998).
 [4] V. Sidis, J. Phys. Chem. **93**, 8128 (1989), and references therein.
 [5] F. Aguillon, V. Sidis, and J. P. Gauyacq, J. Chem. Phys. **95**, 1020 (1991).
 [6] (a) F. Aguillon, Chem. Phys. Lett. **222**, 69 (1994); (b) F. Aguillon, J. Chem. Phys. **109**, 560 (1998).
 [7] D. G. Truhlar and J. T. Muckerman, in *Atom-Molecule Collision Theory*, edited by R. B. Bernstein (Plenum, New York, 1979), p. 505; V. Sidis, Adv. At., Mol., Opt. Phys. **26**, 161 (1990), and references therein.
 [8] U. Saalman and R. Schmidt, Z. Phys. D **38**, 153 (1996).
 [9] F. Aguillon, V. Sidis, and J. P. Gauyacq, Mol. Phys. **81**, 169 (1994).
 [10] M. Sizun and F. Aguillon, Chem. Phys. **177**, 157 (1993); F.

- Aguillon, M. Sizun, V. Sidis, G. D. Billing, and N. Marković, *J. Chem. Phys.* **104**, 4530 (1996).
- [11] F. T. Smith, *Phys. Rev.* **179**, 111 (1969); M. Baer, *Chem. Phys. Lett.* **35**, 112 (1975); M. Baer, *Chem. Phys.* **15**, 49 (1976); V. Sidis, *Adv. Chem. Phys.* **82**, 135 (1992).
- [12] A. E. de Pristo, *J. Chem. Phys.* **79**, 1741 (1983).
- [13] D. A. Babikov (unpublished)
- [14] E. A. Gislason, G. Parlant, and M. Sizun, *Adv. Chem. Phys.* **82**, 423 (1992).
- [15] N. F. Mott and H. S. W. Massey, *The Theory of Atomic Collisions* (Oxford University Press, London, 1965), p. 103.
- [16] C. Courbin-Gaussorgues, P. Wahnon, and M. Barat, *J. Phys. B* **12**, 3047 (1979); C. Courbin-Gaussorgues and V. Sidis, *ibid.* **18**, 699 (1985).
- [17] J. P. Hay and W. R. Wadt, *J. Chem. Phys.* **82**, 270 (1985).
- [18] M. W. Schmidt *et al.*, *J. Comput. Chem.* **14**, 1347 (1993).
- [19] S. Magnier and F. Masnou-Seeuws, *Mol. Phys.* **89**, 711 (1996).
- [20] Carl de Boor, *A Practical Guide to Splines* (Springer-Verlag, New York, 1978); *ACM Trans. Math. Softw.* **5**, 173 (1979).
- [21] D. Dowek, D. Dhuicq, V. Sidis, and M. Barat, *Phys. Rev. A* **26**, 746 (1982); V. Sidis and D. Dowek, in *Electronic and Atomic Collisions*, edited by J. Eichler, I. V. Hertel, and M. Stolterfoht (North-Holland, Amsterdam, 1984), p. 403.